ACS Catalysis

Research Article

Cite This: ACS Catal. 2019, 9, 11447−11454

pubs.acs.org/acscatalysis

Graphene Formation Mechanism by the Electrochemical Promotion of a Ni Catalyst

Juan P. Espinós,[†] Victor J. Rico,[†] Jesús González-Cobos,[‡] Juan R. Sánchez-Valencia,[†] Virginia Pérez-Dieste,[§] Carlos Escudero,[§] Antonio de Lucas-Consuegra,[∥] and Agustín R. González-Elipe*[,†]

[†]Nanotechnology on Surfaces Laboratory, Instituto de Ciencia de Materiales de Sevilla (CSIC-Universidad de Sevilla), Avda. Américo Vespucio 49, 41092 Sevilla, Spain

[‡]Institute of Chemical Research of Catalonia (ICIQ), Ave. Paisos Catalans 16, 43007 Tarragona, Spain

[§]ALBA Synchrotron Light Source, Carres de la Llum 2-26, 08290 Cerdanyola del Vallès, Barcelona, Spain

[∥]Department of Chemical Engineering, School of Chemical Sciences and Technologies, University of Castilla-La Mancha, Avenida Camilo José Cela 12, 13005 Ciudad Real, Spain

Supporting Information

ABSTRACT: In this work, we show that multilayer graphene forms by methanol decomposition at 280 °C on an electrochemically promoted nickel catalyst film supported on a K-βAl_2O_3 solid electrolyte. In operando near ambient pressure photoemission spectroscopy and electrochemical measurements have shown that polarizing negatively the Ni electrode induces the electrochemical reduction and migration of potassium to the nickel surface. This elemental potassium promotes the catalytic decomposition of methanol into graphene and also stabilizes the graphene formed via diffusion and direct K−C interaction. Experiments reveal that adsorbed methoxy radicals are intermediate species in this process and that, once formed, multilayer graphene remains stable after electrochemical oxidation and back migration of potassium to the solid electrolyte upon positive polarization. The reversible diffusion of ca. 100 equivalent monolayers of potassium through the carbon layers and the unprecedented low-temperature formation of graphene and other carbon forms are mechanistic pathways of high potential impact for applications where mild synthesis and operation conditions are required.

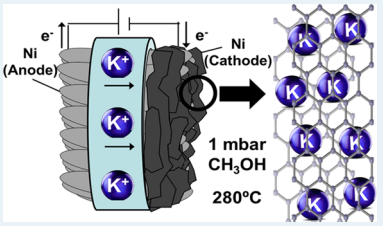

KEYWORDS: *graphene formation, electrocatalysis, nickel electrode, potassium migration, NAP-XPS, methanol decomposition, EPOC*

INTRODUCTION

In the past decade, graphene has been extensively studied due to its outstanding carrier mobility, mechanical strength, flexibility, or chemical properties.[1−4] Graphene synthesis by catalytic decomposition of carbon feed stocks on Cu or Ni takes place at temperatures around 800−1000 °C,[5] which contrasts with the need of reducing the synthesis temperature below 400 °C to integrate graphene as a part of the complementary metal−oxide semiconductor (CMOS) technology.[5] Similar constrains can be quoted for the use of multilayer graphene electrodes in batteries or supercapacitors, where low synthesis and operation temperatures would clearly contribute to increase efficiency.[4,6,7] To release these constrains, the usage of alternative energy-assisted methods (plasma, microwave, or light), the growth on other catalyst surfaces, or the choice of different carbon feed stocks has been proposed as possible solutions to this problem.[8−10] For example, the use of ethanol or methanol is deemed as suitable alternatives because of their lower pyrolysis temperatures and the capacity of OH radicals to etch amorphous carbon. However, despite considerable efforts, the thermal catalytic synthesis of graphene using oxygenated precursors still remains around 850 °C.[11]

The phenomenon of the electrochemical promotion of catalysis (EPOC), discovered by Stoukides and Vayenas in 1981,[12] constitutes an efficient way to enhance gas phase catalytic reaction rates. This phenomenon relies on the electrochemical activation of a catalyst film in contact with a solid electrolyte (e.g., Na^+, K^+, and O^{2-} ionic conductors) that, acting as a source of ions, modifies the surface state of the catalyst electrode and induces a nonfaradaic enhancement of gas phase catalytic activity and a decrease in reaction temperature.[13−16] Incidentally, some EPOC works have also reported an increase in the carbon formation rate as a side reaction during, for example, the steam reforming of CH_4,[17] the CO_2 hydrogenation,[18] or during the methanol wet reforming reaction, the two former using yttria-stabilized zirconia (YSZ; i.e., O^{2-} conductor) and the latter using β-alumina (i.e., K^+ conductor)[19] as solid electrolytes. However, the EPOC phenomenon has never been specifically applied for materials synthesis, an aspect that constitutes the main purpose of the present work aiming at synthesizing multilayer graphene

Received: September 9, 2019
Revised: October 24, 2019
Published: November 5, 2019

DOI: 10.1021/acscatal.9b03820
ACS Catal. 2019, 9, 11447−11454

at low temperatures and to unravel the basic mechanism involved in this process. To this end, a Ni/K-βAl_2O_3/Ni solid electrochemical cell based on nanocolumnar Ni film electrodes has been prepared to promote a catalytic methanol decomposition reaction. Results have shown that multilayer graphene effectively forms at low temperature (280 °C) on the Ni electrode acting as a cathode.

Although some insights on the mechanism of the EPOC phenomenon have been obtained in studies using surface science techniques,[15,20−22] the atomistic understanding of the involved processes is still rather elemental and, in most cases, relies on empirical analysis of electrocatalytic results supported with "ex situ" characterization of the catalysts.[18−20,23,24] More recently, the near ambient pressure XPS (NAP-XPS) technique working "in operando" conditions has demonstrated to be quite useful to understand the EPOC mechanisms and interactions involved in various processes, for example, the role of a Rh catalyst film deposited on yttria-stabilized zirconia (YSZ) (i.e., O^{2-} ionic conductor) in promoting an ethylene−oxygen reaction[24] or the interaction of potassium with the Ni electrode in a Ni/KβAl_2O_3/Au electrocatalytic cell.[25] Herein, we have applied a similar operando approach to study the EPOC decomposition of methanol and the formation mechanism of graphene onto the surface of a similar Ni-catalyst electrode cell. The obtained results have permitted the formulation of an electrochemically promoted nonfaradaic mechanism of carbon formation, in which reduction and diffusion of potassium at the Ni-catalyst film and its involvement in the progressive formation of graphene layers are key features. Since the required operating conditions are clearly milder than those involved in classical catalytic routes of graphene formation,[5,10] the modification of this EPOC methodology might have a high impact in application fields such as batteries or superconductors, where synthesis of carbon electrodes and operation at low temperatures constitute bottle necks of current technologies.[6,7]

RESULTS AND DISCUSSION

Multilayer graphene formation has been proven in a laboratory reactor at atmospheric pressure at 280 °C. Then, the deposition mechanism has been studied by NAP-XPS analysis at reduced pressure conditions and the same temperature. Postreaction Raman analysis has confirmed that similar multilayer graphene formed under these two reaction conditions and that, therefore, the reaction mechanism is general and must be equivalent in the two cases.

EPOC Formation of Graphene in an Electrochemical Cell Reactor at Ambient Pressure. The EPOC formation of graphene was first studied in a double chamber electrochemical cell reactor (probostat) using a Ni/K-βAl_2O_3/Ni solid electrolyte cell that is described in the Methods section. A characteristic of this cell is that the two Ni electrodes are equivalent and have a similar thickness, composition, and microstructure and were fed with the same reaction stream. The scheme of Figure 1a shows that, when a potential of 2 V is applied between the electrodes, potassium migrates toward the cathode. As shown later, these potassium ions are electrochemically reduced at the Ni cathode film and become involved in the formation of carbon via catalytic decomposition of methanol. In fact, in the presence of methanol (163 mbar partial pressure of methanol and Ar as carrier gas) at 280 °C and 1 bar total pressure, a macroscopic black carbon deposit could be observed with a naked eye on the cathode but not on

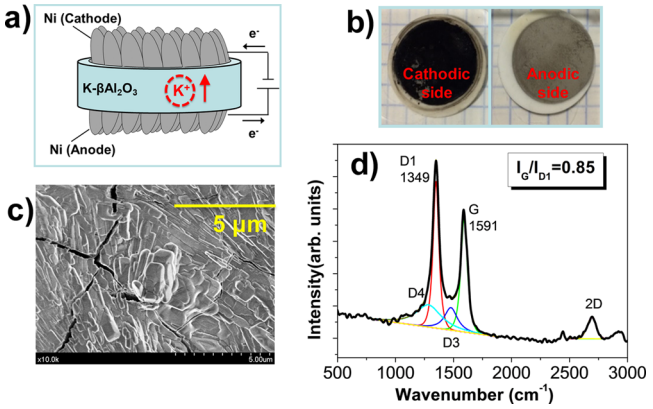

Figure 1. (a) Scheme of the electrochemical cell used in the probostat reactor to prove the EPOC decomposition of methanol. Applying a DC voltage between the Ni electrodes produces the migration of potassium ions from the solid electrolyte to the negatively biased nickel thin film cathode. (b) Images taken by authors of the two sides of an electrolyte pellet with Ni acting as the anode and cathode (i.e., Ni/K-βAl_2O_3/Ni configuration) after the electrocatalytic decomposition of methanol at 280 °C; the side covered with a black coat corresponds to the cathode. (c) Idem SEM image of the carbon deposited onto the Ni electrode by EPOC decomposition of methanol at 280 °C in the probostat setup. (d) Raman spectrum of the same carbon layer.

the anode side of the solid electrochemical cell (Figure 1b). The amount of deposited carbon increased with the running time of the experiment, thus suggesting that it is not a Faradic process. This point will be analyzed in detail in the experiments by NAP-XPS and electrochemical analysis that are discussed below. The carbon deposited on the Ni cathodic film was characterized by scanning electron microscopy (SEM) and Raman spectroscopy analysis. These two techniques confirmed that multilayer graphene had formed on the Ni cathode under the used conditions. Thus, the SEM image in Figure 1c evidences the formation of carbon platelets with a morphology typical of multilayer graphene.[26] Meanwhile, the fitted Raman spectrum in Figure 1d shows two main peaks at 1349 and 1591 cm^{-1} attributed to the D and G modes of graphitic carbon, respectively, the latter due to the C−C bond stretching in graphene and the former due to defects in a graphitic sp^2 structure.[27] A 2D mode at 2687 cm^{-1} supports the formation of multilayered graphene (5−10 layers or less),[27] while its little intensity indicates a high concentration of defects.[28] Another small band at high frequency (2845 cm^{-1}) can be associated with the D + G mode. Overall, the spectrum is consistent with a highly defective nanocrystalline graphene (stage 1, according to Ferrari and Robertson[29]), with an average size of sp^2 graphene around 4.2 nm as deduced from the relative intensity of D and G bands. In addition, fitting analysis in the mild-frequency range according to ref 29. reveals the existence of broad and less intense bands (D2 and D3 located at 1493 and 1226 cm^{-1}, respectively), which can be attributed to amorphous carbon (D2) and C−C and C=C stretching vibrations of polyene-like structures (D3).[29,30] The relatively high concentration of defects in this graphene deposit is consistent with the low temperature used for its synthesis and the fact that increasing the temperature gives rise to carbon nanotubes (CNTs) and other forms of carbon. In fact, although other reaction conditions were not fully explored with this experimental setup, it is noteworthy that changes in the

DOI: 10.1021/acscatal.9b03820
ACS Catal. 2019, 9, 11447−11454

morphology and characteristics of the carbon deposited on the Ni cathode occurred when modifying the reaction temperature. For example, amorphous carbon or even carbon nanotubes (e.g., CNTs decorated at their tip by Ni nanoparticles formed at 420 °C; see Figure S1 in the Supporting Information) were obtained at temperatures above 280 °C. These preliminary results support the high versatility of the EPOC procedure for the fabrication of different forms of carbon materials.

Monitoring of Graphene Formation by NAP-XPS. Monitoring the carbon formation process via the EPOC decomposition of methanol in operando conditions was done at 280 °C in a NAP-XPS instrument using a Ni/K-βAl_2O_3/Au electrochemical cell and low gas pressures (for more details, see the Methods section). Before performing the methanol decomposition experiments, the cell was operated at 280 °C with 10^{-2} mbar water at +2 V Ni electrode polarization to prepare a clean working electrode catalyst surface (this treatment is known to remove any form of previously deposited carbon species as well as any potassium that might have migrated thermally[25]). Then, the atmosphere was switched to 1 mbar methanol at 280 °C under the same potential of +2 V, and the NAP-XPS spectrum in Figure 2a for

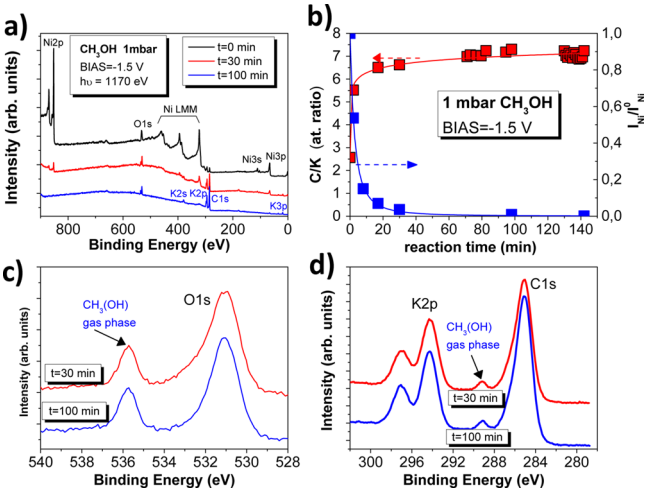

Figure 2. (a) General photoemission spectra taken for the original electrode (t = 0 min) and for the same electrode exposed to methanol at 280 °C for 30 and 100 min while negatively biased at −1.5 V. (b) Plot of the C/K ratio (left axis) determined from the intensity of the C1s and K2p signals and evolution of Ni relative intensity expressed as I_{Ni}/I°_{Ni} as a function of the exposure time to methanol (i.e., reaction time). (c) O1s zone spectra recorded for the electrocatalyst exposed to methanol for 30 and 100 min. (d) Idem for the K2p and C1s spectra.

t = 0 min was recorded. This spectrum depicts intense peaks due to nickel (Ni2p, Ni3p, and Ni Auger peaks), small O1s and C1s features, and a negligible K2p signal, proving that the treatment with water vapor at +2 V h renders a clean reference Ni-catalyst surface that is free of carbon and potassium. Figure 2a also shows the spectra recorded at two successive times when applying a polarization of −1.5 V to the nickel electrode in the presence of 1 mbar methanol. The spectrum taken at t = 30 min reveals an increase in the C1s signal and a drastic decrease of the Ni features, indicating that a thick carbon layer has formed onto the nickel cathode. The evolution with time of the Ni2p peak intensity ratio (denoted as I_{Ni}/I°_{Ni}) presented in Figure 2b confirms that, in this experiment, nickel becomes efficiently covered with carbon after a 20−30 min reaction. Expanded O1s and C1s + K2p spectra in Figure 2c,d shows the formation of a well-defined K2p signal that reaches a steady-state intensity at t > 30 min (see the C/K evolution in Figure 2b). According to their binding energies (BEs), spectra can be attributed to oxygenated carbon species (O1s at 531.35 eV[31−33]), graphitic-like carbon (C1s at 285.30 eV[33−35]), and metallic potassium ($K2p_{3/2}$ at 294.50 eV[36,37]). The presence of two narrow O1s and C1s signals at 536.15 and 289.50 eV, respectively, are attributed to gas phase methanol (this was confirmed in an experiment without a solid sample facing the electron energy analyzer; see Figure S2). As discussed below, the metallic character of potassium is critical for the formation of graphene-like deposits. A quantitative evaluation of the elemental composition derived from the C1s to K2p peak intensities (cf. Figure 2b) yields a 7:1 (C/K) atomic ratio in the steady state for negative polarization of the nickel electrode. Moreover, the initial rapid increase of this C/K ratio and the decrease of Ni peak intensity support the fact that a given amount of potassium ions is electrochemically pumped from the K-βAl_2O_3 electrolyte to the Ni surface (cf. Figure 1a) and that, after reduction to metallic state, it diffuses and becomes incorporated into the progressively grown carbon layers. We propose reaction 1 to describe this potassium reduction, likely at the three-phase boundaries (tpbs) between the electrolyte, the nickel catalyst, and the gas.[25]

$$K^{+}_{(alumina)} + e^{-} \rightarrow K(0)_{(Ni)} \qquad (1)$$

Interestingly, the rapid evolution of current flow measured simultaneously during this experiment (i.e., current varied from −0.6 mA to practically zero after a 0.5 min polarization; see Figure S3) indicates that the potassium reduction at the tpbs takes place sharply during the first seconds of negative polarization. A rough estimation of the total charge flowing through the cell in this initial period of negative polarization gives a value of 1.64 10^{-2} C, which is equivalent to say that approximately 100 equivalent monolayers of potassium migrate from the solid electrolyte to the Ni-catalyst surface.

Since the C1s intensity continued growing for at least 100 min (cf. Figure 2d), the practically constant C/K ratio measured for t > 30 min suggests that the initially pumped and reduced potassium diffuses through the grown carbon deposit, likely contributing to the decomposition of methanol and promoting the continuous formation of carbon in a nonfaradaic process (i.e., without any electrochemical exchange of charge). In the steady state, a homogeneous distribution of potassium in the outmost carbon layers was further confirmed comparing the intensities of K2p and K3p peaks (the latter with a BE of 18.60 eV) recorded with photons of 460 eV and the values of the C1s/K2p peak intensity ratios obtained for two different photon energies of 460 and 1170 eV (see the Supporting Information, Figures S4 and S5). It is also remarkable that a steady-state C/K ratio of 7 (cf. Figure 2b) approaches the ratios, between 6 and 8, found in former studies of potassium and other alkaline metals intercalated into graphite.[36,38] It also suggests that the initially pumped and reduced potassium atoms diffuse and redistribute within the progressively formed carbon layers, in a similar way that evaporated potassium does into graphite at ambient temperature.[36] Migration of alkaline metals through graphene has been also reported and used to induce single-layer graphene delamination from a single crystal metal substrate.[39]

DOI: 10.1021/acscatal.9b03820
ACS Catal. 2019, 9, 11447−11454

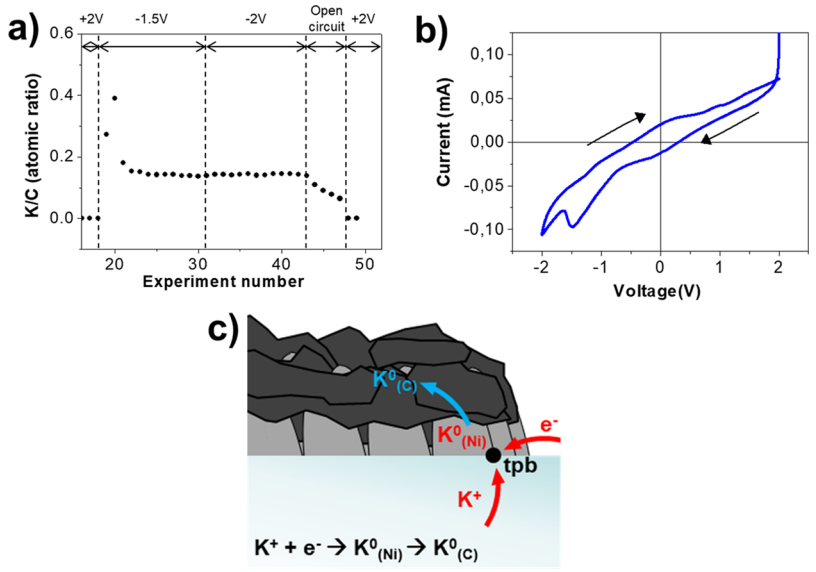

Figure 3. (a) Evolution of the K/C ratio in a series of experiments under negative and positive bias polarization of the nickel electrode during the EPOC decomposition of methanol. (b) Cyclic voltammogram recorded for the electrocatalytic cell once a relatively thick layer of carbon has been formed during the experiments. A similar curve shape could be recorded many times in the presence of methanol in the gas phase. This voltammogram confirms a high reversibility of the electrochemical processes induced in the cell, entailing the reduction/oxidation of potassium (see main text). (c) Scheme describing the out forward and backward diffusion of potassium from the electrolyte up to the outer graphene layers and its reduction/oxidation at the tpbs under negative and positive polarizations, respectively.

According to the plot in Figure 3a, the K/C ratio remained invariant for long times under negative polarization but rapidly decreased when changing the bias voltage to positive. This means that the electrochemical reaction 1 is fully reversible when switching the polarization of the nickel electrode to positive, a process that must be attributed to the electrochemical oxidation (likely at the tpb) and back migration of potassium ions to the K-βAl_2O_3 solid electrolyte. This forward/backward migration of potassium occurred both in the presence and the absence of methanol and was further analyzed by cyclic voltammetry measurements carried out during the EPOC operation in the same NAP-XPS cell. The *I*−*V* voltammogram in Figure 3b confirms both the opposite sign of the current flowing through the cell when changing the polarization and the similar magnitude of electric charge transferred during the negative (−34 mC) and positive (29 mC) polarizations in this cyclic voltammetry experiment. These experimental evidence shed some light into the basic mechanism of the EPOC process, leading to the formation of graphene that can be schematized by the drawings in Figure 3c and reactions 2−4 below.

$$CH_3OH + Ni(K) \rightarrow C - Ni(K) + H_2O + H_2 \quad (2)$$

$$C - Ni(K) \rightarrow C(K) - Ni \quad (3)$$

$$CH_3OH + C(K) - Ni \rightarrow C - C(K) - Ni + H_2O + H_2 \quad (4)$$

They describe the potassium-promoted catalytic formation of carbon deposits through several successive steps. The first one is the already mentioned migration and electrochemical reduction of a given amount of potassium ions at the nickel surface under negative polarization (reaction 1). These potassium atoms adsorbed on the nickel surface activate the catalytic decomposition of methanol and the formation of the first graphene layers (reaction 2). Potassium atoms then diffuse through the graphene (reaction 3), where they distribute homogeneously in its outmost surface layers (i.e., in a C/K ratio around 7) and continues promoting the catalytic methanol decomposition (reaction 4).

In this scheme, potassium is essential to promote the catalytic decomposition of methanol and the formation and stabilization of carbon as multilayer graphene. The formation of this form of carbon during the NAP-XPS experiment was also confirmed by Raman analysis (see the Supporting Information, Figure S6) and agrees with a previous work on the EPOC wet reforming of methanol, showing that, besides CO and H_2 as main reaction products, a small amount of carbon formed as a subproduct.[23] The present results show that reactions 2−4 prevail in the absence of water and lead to the formation of thick carbon deposits.

Intermediate Species and Graphene Formation Mechanism. Additional information about the graphene formation mechanism was gained by analyzing the O1s and C1s peaks recorded during the experiment. Figure 4 shows the fitted O1s and C1s (plus K2p) spectra recorded in the presence of methanol while sequentially biasing the electrode at −2 and +2 V and then, after purging the methanol, at this latter polarization. At −2 V (Figure 4a), the O1s spectrum depicts a relatively narrow band at 535.9 eV attributed to gas phase methanol (see Figure S2) and a high intensity band (IV) at 531.3 eV tentatively attributed to adsorbed methoxy-like species.[31−33] A tail around 532.4 eV (band II) is likely due to a more oxidized C1 species (e.g., deprotonated formaldehyde and/or formic acid). At −2 V, fitting the C1s signal requires an intense peak at 285.3 due to graphitic-like carbon[35] and two small bands at around 286.6−288.0 eV that can be attributed to the methoxy-like species monitored at the O1s spectrum.[33] An intense K2p signal attributed to metallic potassium[36,37] complies with the aforementioned C/K = 7 intensity ratio. Methoxy species are commonly claimed as intermediate species in the catalytic decomposition and steam reforming of methanol.[40,41] In the absence of water, the NAP-XPS

DOI: 10.1021/acscatal.9b03820
ACS Catal. 2019, 9, 11447−11454

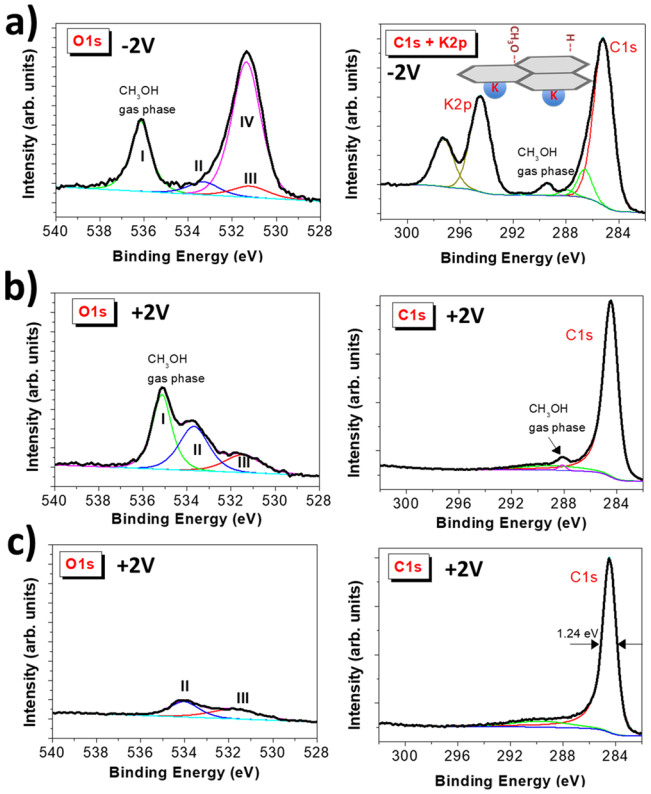

Figure 4. (a) O1s (left) and K2p + C1s (right) fitted spectra recorded during the EPOC-activated deposition of carbon according to reactions 2−4 while applying a bias potential of −2 V. The inset of this figure shows the scheme illustrating the dissociative adsorption of methanol activated by C(K) sites. (b) O1s (left) and K2p + C1s (right) fitted spectra recorded while applying a bias potential of +2 V. (c) O1s (left) and K2p + C1s (right) fitted spectra recorded when sequentially removing the methanol from the gas phase.

detection of methoxy-like species (cf. Figure 4a) suggests a methanol adsorption and dissociation mechanism according to reaction 5 below and the scheme in the inset of Figure 4

$$CH_3OH + C(K) - Ni \rightarrow [CH_3O \cdots C(K) \cdots H] - Ni \quad (5)$$

This scheme and reaction represent a separated covalent adsorption of methoxy and hydrogen radicals onto the potassium-activated carbon, an adsorption state that agrees with literature results reporting the adsorption of methoxy species on graphite[42] and that of atomic hydrogen on potassium-intercalated graphite.[43,44] Although no direct NAP-XPS evidence were obtained of other intermediate species resulting from the decomposition of methoxy moieties, we propose that carbon results from their decomposition when mediated by potassium atoms that, interacting with the already formed graphene, contribute to its stabilization through a direct K−C interaction. Numerous theoretical and experimental works have shown that, when alkaline atoms are intercalated in graphite or interact with graphene, there is a transfer of charge toward the carbon structure, modifying its density of charge and stabilizing the system.[38,45,46] Although we cannot rule out the growth of graphene layers by methanol/methoxy decomposition onto gas-accessible nickel electrode sites (reaction 2), the simultaneous detection of methoxy groups onto the outermost graphene layers together with potassium interacting with the graphene supports that the active sites of the EPOC process involve these potassium atoms located in the outer layers of deposited carbon (cf. scheme in Figure 4a).

NAP-XPS spectra recorded after changing the polarization from −2 to +2 V (cf. Figure 4b) provided clear evidence of the need of negative polarization to induce the formation of graphene and therefore support a methanol decomposition mechanism based on reactions 1−5. At +2 V, spectra consisted of a O1s signal with three bands: band (I) at 535.10 eV due to gaseous methanol (note that its apparent binding energy is affected by the voltage applied to the electrode), band (II) at 533.60 eV assigned to highly oxidized C1 adsorbed species (e.g., dehydrogenated formic acid or formaldehyde[40]), and band (III) at 531.45 eV due to remaining traces of methoxy-like species. Simultaneously, the K2p + C1s spectral regions showed the complete disappearance of the K2p signal (reverse reaction 1) and a narrowing of the C1s band from 1.90 eV FWHM at −2 V to 1.24 eV at +2 V. The appearance of a small broad contribution around 288 eV is likely due to the oxidized carbon species in compliance with the O1s band analysis and/or to a C1s plasmon feature. Following previous studies of potassium evaporated on a single crystalline graphite,[36] the FWHM broadening in the presence of potassium is due to the development of an intense electronic interaction between elemental potassium and graphitic-like carbon.[38,45,46] A similar behavior regarding the removal of potassium, the formation of oxidized carbon species, and the narrowing of the graphitic peak can be deduced from Figure 4c after pumping out the methanol at +2 V, while residual oxidized carbon species (II) and (III) remained adsorbed onto the carbon surface. A rough estimate from the C1s and O1s spectra in this figure of the amount of oxygen present in this sample yields an O/C ratio of 0.016, indicating that, although some oxygen might remain in the formed graphene, its concentration is relatively low.

Additional NAP-XPS experiments with water and oxygen at 280 °C at +2 V showed that the deposited carbon was rather stable. No changes occurred at 280 °C in the presence of 0.5 mbar water vapor, although partial removal took place at 2 mbar. Complete carbon removal occurred with 1 mbar oxygen (see the Supporting Information, Figure S7). These experiments have also proven the metallic state of potassium during the formation of graphene since, upon oxidation, the K2p peak shifted to 293.55 eV (Figure S7), the typical BE of potassium in cationic form.[47]

Carbon formed through reactions 1−5 during the NAP-XPS experiments was ex situ characterized by Raman spectroscopy. The recorded spectrum corresponding to a carbon layer resulting from low-pressure methanol decomposition for 100 min in the synchrotron line was rather similar (see the Supporting Information, Figure S6) to that formed in the laboratory probostat electrochemical cell reactor at atmospheric pressure (Figure 1d). This equivalence of results supports that the potassium promotion of reactions 2−5 is essential for grapheme formation. From a synthetic point of view, the mild operation temperatures required for multilayer graphene formation using the EPOC technique clearly outperforms current catalytic processes[5,11] and may be of potential interest for the direct fabrication of carbon electrodes, a possibility that will be explored in future studies.

CONCLUSIONS

In this work, we have proven that multilayer graphene forms at relatively low temperatures using an EPOC system consisting

DOI: 10.1021/acscatal.9b03820
ACS Catal. 2019, 9, 11447−11454

of a K-βAl_2O_3 solid electrolyte and a nickel catalyst acting as the cathode. Studying the mechanism of graphene formation under operando conditions by NAP-XPS, we have shown that potassium ions from the electrolyte migrate and become electrochemically reduced at the Ni surface. Then, atomic potassium diffuses through the progressively formed graphene layers, acting as the promoter of the catalytic decomposition of methanol at 280 °C. We attribute the effectiveness of this process to (i) a double role of potassium as a promoter for the catalytic decomposition of methanol and a stabilizer of the graphene structure and (ii) the diffusion of metallic potassium through the multilayer graphene toward its surface where it contributes to the stabilization of graphene and the dissociative adsorption of methanol. Features (i) and (ii) and the electrochemically driven reversible supply/removal of potassium and its stabilization in the multilayer graphene represent unique features of the investigated EPOC procedure with a large prospect of application in electrochemical-driven systems such as electrocatalysis, ion batteries, or supercapacitors, where mild synthesis conditions for the carbon electrodes can be advantageous for operation.

METHODS

Electrocatalytic methanol decomposition experiments were first carried out in a double chamber electrochemical cell reactor (probostat reactor) setup previously described in ref 48. The same reaction gas mixture consisting of an Ar flow (100 sccm) bubbled through a methanol saturator at ambient temperature was fed to both sides of the cell. The saturated gas stream had a 163 mbar partial pressure of methanol. Graphene formation experiments were typically performed at 280 °C under a polarization of 2 V between the two electrodes. Additional experiments were also carried out at increasing temperatures. The preparation procedure and structure of the solid electrolyte system utilized in this experiment is similar to those utilized in a previous work dealing with the EPOC reforming reaction of methanol.[23] Basically, it consisted of a nanostructured nickel film deposited by electron beam evaporation at oblique angles (80°)[23,25,49] on both sides of a 19 mm-diameter, 1 mm-thick K-βAl_2O_3 (Ionotec) electrolyte disc (i.e., Ni/K-βAl_2O_3/Ni configuration, where nickel acts either as the cathode or anode). As determined by Rutherford backscattering spectroscopy (RBS) analysis, the equivalent mass thickness (i.e., assuming a dense and compact layer) of the nanostructured Ni thin films was 900 nm. A complete characterization analysis of the nanocolumnar structure of these thin films and of their catalytic/electrocatalytic behavior for methanol wet reforming can be found in these previous works.[23,25] From this analysis, it is of relevance for the present investigation that the nanostructured Ni thin film electrode covers completely the alumina electrolyte disc and depicts nanocolumnar patches with high porosity and effective exposed area.

The preparation procedure and structure of the solid electrolyte cell utilized for the NAP-XPS experiments was similar to those used in the probostat. On one side, it incorporated as a working electrode (W), the same Ni nanostructured film utilized for the probostat cell reactor. A catalytically inert gold counter/reference (C/R) electrode was deposited on the other side of the electrolyte disc (i.e., according to a Ni/K-βAl_2O_3/Au configuration). For the NAP-XPS experiments, the Ni/K-βAl_2O_3/Au electrocatalytic cell was incorporated in a specially designed stainless steel sample holder with the back face covered with gold glued with silver paste. The two poles of the cell were connected with a silver thread to a potentiostat/galvanostat (Vertex model, Ivium Technologies) to electrically operate the system. The exposed area available for reaction was 2.01 cm^2. A complete description of this holder can be found in ref 25. To apply the operating voltage, the nickel electrode was connected to the galvanostat supply and to the ground. In this way, the earthed Ni electrode presented a constant reference level to accurately measure the BEs of the photoelectron spectra. The convention in the text when talking about positive and negative polarizations of the nickel electrode refers to the potential difference with respect to the gold electrode that, for these two situations, was negatively and positively polarized with respect to the ground.

The NAP-XPS experiments were performed at the end station of the BL-24 CIRCE undulator beamline in the ALBA synchrotron light source (Cerdanyola del Vallès, Spain). The NAP-XPS station has a commercial Phoibos NAP150 XPS analyzer (SPECS). The beam spot was around 100 × 150 μm^2. Most spectra were collected upon excitation with photons of 1170 eV using a pass energy in the spectrometer of 10 eV. Some spectra were also recorded with 460 eV photons as indicated in the text and in the Supporting Information. Surface atomic composition and ratios were determined from the areas of the K2p, C1s, K2p, Ni2p, and Ni3p spectra measured at the two photon energies and considering the corresponding cross sections[50] and scape depth of photoelectrons.[51] All experiments were carried out at 280 °C. Reaction atmospheres, at pressures in the order of 1 mbar (see main text), consisted of pure methanol, water, or oxygen, depending on experiments. The residual pressure in the chamber after dosing these vapors and gases was 10^{-7} mbar.

Before performing the EPOC methanol decomposition experiments, the cell was operated at 280 °C in the presence of 10^{-2} mbar water. As reported in a previous work, this pretreatment is quite efficient to remove any form of carbon, including adventitious contamination, previously deposited on the electrocatalyst surface. The Ni electrode was also polarized at +2 V for almost 1 h before starting the methanol decomposition experiments to ensure that the Ni film as a reference state is free of potassium.[25]

After the electrocatalytic operation experiments both in the probostat and in the NAP-XPS cell, the surface of the electrodes was examined by scanning electron microscopy (SEM) and Raman spectroscopy to determine the characteristics of the carbon deposits formed on the surface of the nickel electrode. SEM images were taken with a field emission microscope (FESEM model Hitachi S4800) at the Instituto de Ciencia de Materiales de Sevilla, CSIC-US, Seville, Spain. Raman analysis of the carbon deposits was carried out in a LabRAM HR high-resolution 800 confocal Raman microscope. A green laser (He−Ne 532.14 mn), 600 line/mm, 100× objective, 20 mW, and 100 μ pinhole, was employed for the measurements.

ASSOCIATED CONTENT

Supporting Information

The Supporting Information is available free of charge on the ACS Publications website at DOI: 10.1021/acscatal.9b03820.

Evidence of the formation of CNTs at high temperatures, photoelectron spectra of gas phase methanol, an

DOI: 10.1021/acscatal.9b03820
ACS Catal. 2019, 9, 11447−11454

analysis of the evolution of current intensity with time during cathodic polarization, NAP-XPS of the distribution of potassium within the carbon deposit, Raman spectrum of the surface of the cell used for the NAP-XPS experiments, and results on the chemical reactivity of electrocatalytically deposited carbon (PDF)

AUTHOR INFORMATION

Corresponding Author

*E-mail: arge@icmse.csic.es.

ORCID

Juan P. Espinós: 0000-0002-3053-0841
Victor J. Rico: 0000-0002-5083-0390
Carlos Escudero: 0000-0001-8716-9391
Antonio de Lucas-Consuegra: 0000-0001-8080-8293
Agustín R. González-Elipe: 0000-0002-6417-1437

Notes

The authors declare no competing financial interest.

ACKNOWLEDGMENTS

We thank the CSIC (201860E050), the AEI-MINECO (MAT2016-79866-R), and the EU through cohesion fund and FEDER programs for financial support. J.R.S.-V. thanks the University of Seville through the VI PPIT-US and MINECO for the "Ramon y Cajal" national program.

REFERENCES

(1) Geim, A. K.; Novoselov, K. S. The Rise of Graphene. *Nat. Mater.* **2007**, *6*, 183−191.
(2) Liao, L.; Peng, H.; Liu, Z. Chemistry Makes Graphene beyond Graphene. *J. Am. Chem. Soc.* **2014**, *136*, 12194−12200.
(3) Wu, J.-B.; Lin, M.-L.; Cong, X.; Liu, H.-N.; Tan, P.-H. Raman Spectroscopy of Graphene-Based Materials and Its Applications in Related Devices. *Chem. Soc. Rev.* **2018**, *47*, 1822−1873.
(4) Lv, T.; Liu, M.; Zhu, D.; Gan, L.; Chen, T. Nanocarbon-Based Materials for Flexible All-Solid-State Supercapacitors. *Adv. Mater.* **2018**, *30*, 1705489.
(5) Son, M.; Ham, M.-H. Low-Temperature Synthesis of Graphene by Chemical Vapor Deposition and Its Applications. *FlatChem* **2017**, *5*, 40−49.
(6) Kumar, R.; Joanni, E.; Singh, R. K.; Singh, D. P.; Moshkalev, S. A. Recent Advances in the Synthesis and Modification of Carbon-Based 2D Materials for Application in Energy Conversion and Storage. *Prog. Energy Combust. Sci.* **2018**, *67*, 115−157.
(7) Kim, Y.; Kim, J.-K.; Vaalma, C.; Bae, G. H.; Kim, G.-T.; Passerini, S.; Kim, Y. Optimized Hard Carbon Derived from Starch for Rechargeable Seawater Batteries. *Carbon* **2018**, *129*, 564−571.
(8) Lee, J.; Han, T.-H.; Park, M.-H.; Jung, D. Y.; Seo, J.; Seo, H.-K.; Cho, H.; Kim, E.; Chung, J.; Choi, S.-Y.; Kim, T.-S.; Lee, T.-W.; Yoo, S. Synergetic Electrode Architecture for Efficient Graphene-Based Flexible Organic Light-Emitting Diodes. *Nat. Commun.* **2016**, *7*, 11791.
(9) Muñoz, R.; Martínez, L.; López-Elvira, E.; Munuera, C.; Huttel, Y.; García-Hernández, M. Direct Synthesis of Graphene on Silicon Oxide by Low Temperature Plasma Enhanced Chemical Vapor Deposition. *Nanoscale* **2018**, *10*, 12779−12787.
(10) Guo, L.; Zhang, Z.; Sun, H.; Dai, D.; Cui, J.; Li, M.; Xu, Y.; Xu, M.; Du, Y.; Jiang, N.; Huang, F.; Lin, C.-T. Direct Formation of Wafer-Scale Single-Layer Graphene Films on the Rough Surface Substrate by PECVD. *Carbon* **2018**, *129*, 456−461.
(11) Guermoune, A.; Chari, T.; Popescu, F.; Sabri, S. S.; Guillemette, J.; Skulason, H. S.; Szkopek, T.; Siaj, M. Chemical Vapor Deposition Synthesis of Graphene on Copper with Methanol, Ethanol, and Propanol Precursors. *Carbon* **2011**, *49*, 4204−4210.
(12) Stoukides, M.; Vayenas, C. G. The Effect of Electrochemical Oxygen Pumping on the Rate and Selectivity of Ethylene Oxidation on Polycrystalline Silver. *J. Catal.* **1981**, *70*, 137−146.
(13) Vayenas, C. G.; Bebelis, S.; Pliangos, C.; Brosda, S.; Tsiplakides, D. *Electrochemical Activation of Catalysis: Promotion, Electrochemical Promotion, and Metal-Support Interactions*; Springer US: 2001.
(14) González-Cobos, J.; Valverde, J. L.; de Lucas-Consuegra, A. Electrochemical vs. Chemical Promotion in the H_2 Production Catalytic Reactions. *Int. J. Hydrogen Energy* **2017**, *42*, 13712−13723.
(15) Lambert, R. M.; Tikhov, M.; Palermo, A.; Yentekakis, I. V.; Vayenas, C. G. Electrochemical Promotion of Environmentally Important Catalytic Reactions. *Ionics* **1995**, *1*, 366−376.
(16) Vernoux, P.; Lizarraga, L.; Tsampas, M. N.; Sapountzi, F. M.; De Lucas-Consuegra, A.; Valverde, J.-L.; Souentie, S.; Vayenas, C. G.; Tsiplakides, D.; Balomenou, S.; Baranova, E. A. Ionically Conducting Ceramics as Active Catalyst Supports. *Chem. Rev.* **2013**, *113*, 8192−8260.
(17) Yentekakis, I. V.; Jiang, Y.; Neophytides, S.; Bebelis, S.; Vayenas, C. G. Catalysis, Electrocatalysis and Electrochemical Promotion of the Steam Reforming of Methane over Ni Film and Ni-YSZ Cermet Anodes. *Ionics* **1995**, *1*, 491−498.
(18) Ruiz, E.; Martínez, P. J.; Morales, Á.; San Vicente, G.; de Diego, G.; Sánchez, J. M. Electrochemically Assisted Synthesis of Fuels by CO_2 Hydrogenation over Fe in a Bench Scale Solid Electrolyte Membrane Reactor. *Catal. Today* **2016**, *268*, 46−59.
(19) González-Cobos, J.; López-Pedrajas, D.; Ruiz-López, E.; Valverde, J. L.; de Lucas-Consuegra, A. Applications of the Electrochemical Promotion of Catalysis in Methanol Conversion Processes. *Top. Catal.* **2015**, *58*, 1290−1302.
(20) González-Cobos, J.; De Lucas-Consuegra, A. A Review of Surface Analysis Techniques for the Investigation of the Phenomenon of Electrochemical Promotion of Catalysis with Alkaline Ionic Conductors. *Catalysts* **2016**, *6*, 15.
(21) Williams, F. J.; Palermo, A.; Tikhov, M. S.; Lambert, R. M. The Origin of Electrochemical Promotion in Heterogeneous Catalysis: Photoelectron Spectroscopy of Solid State Electrochemical Cells. *J. Phys. Chem. B* **2000**, *104*, 615−621.
(22) Williams, F. J.; Tikhov, M. S.; Palermo, A.; Macleod, N.; Lambert, R. M. Electrochemical Promotion of Rhodium-Catalyzed NO Reduction by CO and by Propene in the Presence of Oxygen. *J. Phys. Chem. B* **2001**, *105*, 2800−2808.
(23) González-Cobos, J.; Rico, V. J.; González-Elipe, A. R.; Valverde, J. L.; de Lucas-Consuegra, A. Electrocatalytic System for the Simultaneous Hydrogen Production and Storage from Methanol. *ACS Catal.* **2016**, *6*, 1942−1951.
(24) Katsaounis, A.; Teschner, D.; Zafeiratos, S. The Effect of Polarization and Reaction Mixture on the Rh/YSZ Oxidation State During Ethylene Oxidation Studied by Near Ambient Pressure XPS. *Top. Catal.* **2018**, *61*, 2142−2151.
(25) Espinós, J. P.; Rico, V. J.; González-Cobos, J.; Sánchez-Valencia, J. R.; Pérez-Dieste, V.; Escudero, C.; de Lucas-Consuegra, A.; González-Elipe, A. R. In Situ Monitoring of the Phenomenon of Electrochemical Promotion of Catalysis. *J. Catal.* **2018**, *358*, 27−34.
(26) Wang, F.; Drzal, L. T.; Qin, Y.; Huang, Z. Processing and Characterization of High Content Multilayer Graphene/Epoxy Composites with High Electrical Conductivity. *Polym. Compos.* **2016**, *37*, 2897−2906.
(27) Ferrari, A. C.; Basko, D. M. Raman Spectroscopy as a Versatile Tool for Studying the Properties of Graphene. *Nat. Nanotechnol.* **2013**, *8*, 235−246.
(28) Malard, L. M.; Pimenta, M. A.; Dresselhaus, G.; Dresselhaus, M. S. Raman Spectroscopy in Graphene. *Phys. Rep.* **2009**, *473*, 51−87.
(29) Ferrari, A. C.; Robertson, J. Interpretation of Raman Spectra of Disordered and Amorphous Carbon. *Phys. Rev. B* **2000**, *61*, 14095−14107.
(30) Cabello, M.; Chyrka, T.; Klee, R.; Aragón, M. J.; Bai, X.; Lavela, P.; Vasylchenko, G. M.; Alcántara, R.; Tirado, J. L.; Ortiz, G. F. Treasure Na-Ion Anode from Trash Coke by Adept Electrolyte Selection. *J. Power Sources* **2017**, *347*, 127−135.

DOI: 10.1021/acscatal.9b03820
ACS Catal. 2019, 9, 11447−11454

(31) Tanaka, K.; Matsuzaki, S.; Toyoshima, I. Photodecomposition of Adsorbed Methoxy Species by UV Light and Formaldehyde Adsorption on Silicon(111) Studied by XPS and UPS. *J. Phys. Chem.* **1993**, *97*, 5673−5677.
(32) Worley, S. D.; Erickson, N. E.; Madey, T. E.; Yates, J. T., Jr. An XPS Study of Formaldehyde and Related Molecules Adsorbed on the Surface of a Tungsten (100) Single Crystal. *J. Electron Spectrosc. Relat. Phenom.* **1976**, *9*, 355−370.
(33) Hueso, J. L.; Espinós, J. P.; Caballero, A.; Cotrino, J.; González-Elipe, A. R. XPS Investigation of the Reaction of Carbon with NO, O_2, N_2 and H_2O Plasmas. *Carbon* **2007**, *45*, 89−96.
(34) Koinuma, M.; Tateishi, H.; Hatakeyama, K.; Miyamoto, S.; Ogata, C.; Funatsu, A.; Taniguchi, T.; Matsumoto, Y. Analysis of Reduced Graphene Oxides by X-Ray Photoelectron Spectroscopy and Electrochemical Capacitance. *Chem. Lett.* **2013**, *42*, 924−926.
(35) Batra, A.; Cvetko, D.; Kladnik, G.; Adak, O.; Cardoso, C.; Ferretti, A.; Prezzi, D.; Molinari, E.; Morgante, A.; Venkataraman, L. Probing the Mechanism for Graphene Nanoribbon Formation on Gold Surfaces through X-Ray Spectroscopy. *Chem. Sci.* **2014**, *5*, 4419−4423.
(36) Caballero, A.; Espinós, J. P.; Fernández, A.; Soriano, L.; González-Elipe, A. R. Adsorption and Oxidation of K Deposited on Graphite. *Surf. Sci.* **1996**, *364*, 253−265.
(37) Wilde, M.; Beauport, I.; Stuhl, F.; Al-Shamery, K.; Freund, H.-J. Adsorption of Potassium on Cr_2O_3(0001) at Ionic and Metallic Coverages and Uv-Laser-Induced Desorption. *Phys. Rev. B* **1999**, *59*, 13401−13412.
(38) Algdal, J.; Balasubramanian, T.; Breitholtz, M.; Kihlgren, T.; Walldén, L. Thin Graphite Overlayers: Graphene and Alkali Metal Intercalation. *Surf. Sci.* **2007**, *601*, 1167−1175.
(39) Palacio, I.; Aballe, L.; Foerster, M.; Oteyza, D. G.; de García-Hernández, M.; Martín-Gago, J. A. Reversible Graphene Decoupling by NaCl Photo-Dissociation. *2D Mater.* **2019**, *6*, No. 025021.
(40) Zhou, Y.-H.; Lv, P.-H.; Wang, G.-C. DFT Studies of Methanol Decomposition on Ni(100) Surface: Compared with Ni(111) Surface. *J. Mol. Catal. A: Chem.* **2006**, *258*, 203−215.
(41) Yong, S. T.; Ooi, C. W.; Chai, S. P.; Wu, X. S. Review of Methanol Reforming-Cu-Based Catalysts, Surface Reaction Mechanisms, and Reaction Schemes. *Int. J. Hydrogen Energy* **2013**, *38*, 9541−9552.
(42) Schröder, E. Methanol Adsorption on Graphene. *J. Nanomater.* **2013**, *2013*, 1−6.
(43) *Graphite Intercalation Compounds II: Transport and Electronic Properties*; Zabel, H., Solin, S. A., Eds.; Springer Series in Materials Science; Springer-Verlag: Berlin Heidelberg, 1992.
(44) Deng, W.-Q.; Xu, X.; Goddard, W. A. New Alkali Doped Pillared Carbon Materials Designed to Achieve Practical Reversible Hydrogen Storage for Transportation. *Phys. Rev. Lett.* **2004**, *92*, 166103.
(45) Ahmad, S.; Miró, P.; Audiffred, M.; Heine, T. Tuning the Electronic Structure of Graphene through Alkali Metal and Halogen Atom Intercalation. *Solid State Commun.* **2018**, *272*, 22−27.
(46) Kamakura, N.; Kubota, M.; Ono, K. Band Dispersion and Bonding Character of Potassium on Graphite. *Surf. Sci.* **2008**, *602*, 95−101.
(47) Joseph, Y.; Ketteler, G.; Kuhrs, C.; Ranke, W.; Weiss, W.; Schlögl, R. On the Preparation and Composition of Potassium Promoted Iron Oxide Model Catalyst Films. *Phys. Chem. Chem. Phys.* **2001**, *3*, 4141−4153.
(48) Garcia-Garcia, F. J.; Beltrán, A. M.; Yubero, F.; González-Elipe, A. R.; Lambert, R. M. High Performance Novel Gadolinium Doped Ceria/Yttria Stabilized Zirconia/Nickel Layered and Hybrid Thin Film Anodes for Application in Solid Oxide Fuel Cells. *J. Power Sources* **2017**, *363*, 251−259.
(49) Barranco, A.; Borras, A.; Gonzalez-Elipe, A. R.; Palmero, A. Perspectives on Oblique Angle Deposition of Thin Films: From Fundamentals to Devices. *Prog. Mater. Sci.* **2016**, *76*, 59−153.
(50) Scofield, J. H. Hartree-Slater Subshell Photoionization Cross-Sections at 1254 and 1487 EV. *J. Electron Spectrosc. Relat. Phenom.* **1976**, *8*, 129−137.
(51) Tanuma, S.; Powell, C. J.; Penn, D. R. Calculations of Electron Inelastic Mean Free Paths. IX. Data for 41 Elemental Solids over the 50 EV to 30 KeV Range. *Surf. Interface Anal.* **2011**, *43*, 689−713.

DOI: 10.1021/acscatal.9b03820
ACS Catal. 2019, 9, 11447−11454